Title

MicroED structure of lipid-embedded mammalian mitochondrial voltage-dependent anion channel

Journal

Proceedings of the National Academy of Sciences of the United States of America, 117(51)

ISSN

0027-8424

Authors

Martynowycz, Michael W
Khan, Farha
Hattne, Johan
et al.

Publication Date

2020-12-22

DOI

10.1073/pnas.2020010117

Peer reviewed

MicroED structure of lipid-embedded mammalian mitochondrial voltage-dependent anion channel

Michael W. Martynowycz[a,b], Farha Khan[c], Johan Hattne[a,b], Jeff Abramson[c], and Tamir Gonen[a,b,c,1]

[a]Howard Hughes Medical Institute, University of California, Los Angeles, CA 90095; [b]Department of Biological Chemistry, University of California, Los Angeles, CA 90095; and [c]Department of Physiology, University of California, Los Angeles, CA 90095

Edited by Yifan Cheng, University of California, San Francisco, CA, and approved November 8, 2020 (received for review September 24, 2020)

A structure of the murine voltage-dependent anion channel (VDAC) was determined by microcrystal electron diffraction (MicroED). Microcrystals of an essential mutant of VDAC grew in a viscous bicelle suspension, making it unsuitable for conventional X-ray crystallography. Thin, plate-like crystals were identified using scanning-electron microscopy (SEM). Crystals were milled into thin lamellae using a focused-ion beam (FIB). MicroED data were collected from three crystal lamellae and merged for completeness. The refined structure revealed unmodeled densities between protein monomers, indicative of lipids that likely mediate contacts between the proteins in the crystal. This body of work demonstrates the effectiveness of milling membrane protein microcrystals grown in viscous media using a focused ion beam for subsequent structure determination by MicroED. This approach is well suited for samples that are intractable by X-ray crystallography. To our knowledge, the presented structure is a previously undescribed mutant of the membrane protein VDAC, crystallized in a lipid bicelle matrix and solved by MicroED.

cryoEM | MicroED | bicelle crystallization | FIB/SEM | microcrystal electron diffraction

Resolving crystal structures of membrane proteins is challenging. In contrast to soluble proteins, membrane proteins have both hydrophobic and hydrophilic regions on their surface, making them difficult to purify and crystallize. A bottleneck in traditional X-ray crystallography is growing large, well-ordered crystals of membrane proteins that incorporate ordered or semiordered lipids. To overcome this, membrane proteins are frequently solubilized with detergent, which often displaces protein-embedded lipids that play critical roles in their structure and function (1). For this reason, several methods have been developed for crystallizing membrane proteins within a lipid matrix, for example, lipidic cubic phase (LCP) and bicelles (2–5). Viscous media such as lipids or lipid/detergent mixtures are used to mimic the hydrophobic environment of a lipid bilayer. This viscous medium is problematic for traditional cryoelectron microscopy (cryoEM) blotting methods. In an attempt to circumvent these limitations, investigators have utilized nanoliter deposition through pin printing (6), vacuuming away the excess media using a pressure differential (7), liquid wicking grids (8), and changing the phase of the media using other less viscous detergents (9). Although these approaches have been successful for soluble protein crystals, there has been little progress for membrane protein crystals, likely stemming from crystal dehydration or damaging the crystal lattice. To prevent this, it is preferable to leave membrane protein crystals in their mother liquor and freeze them as quickly as possible to preserve their hydration state and crystalline order.

To date, $Ca^{2+/}$ ATPase (10) and the nonselective ion channel NaK (11) have been solved by microcrystal electron diffraction (MicroED). Ca^{2+} ATPase crystals were grown using dialysis of isolated protein against detergent-free buffer. Ordered two-dimensional (2D) layers of lipid-$Ca^{2+/}$ ATPase formed and slowly began to stack, resulting in thin three-dimensional (3D) crystals. These submicron crystals were only a few layers thick, making them suitable for analysis by MicroED, but they represent a special case where 3D crystals formed serendipitously from stacked 2D crystals. Moreover, this crystallization method requires large amounts of purified protein, and the crystallization technique is slow and laborious. In sharp contrast, microcrystals of NaK were identified in conditions using detergents out of a sparse matrix. The crystals formed as small cubes containing approximately 1,000 diffracting units. These crystals grew out of a detergent solution, without any lipids; they were easy to pipette, and excess solution blotted easily for cryoEM grid preparation using standard vitrification equipment (12). In both examples, the resulting crystals were thinner than about 500 nm, making both sample preparation and data collection straightforward. However, it is preferable to study membrane proteins with lipids rather than in detergent (13). Crystallization of membrane proteins in LCP or in lipid bicelles regularly yields crystals in the 1 to 5 μm range, which are too small for traditional X-ray crystallography and too large for MicroED. Moreover, the thick lipid matrix renders such samples almost impossible to prepare by traditional blotting methods for cryoEM, because the lipid matrix is viscous and integrated into the crystal. If blotting is inefficient, the sample becomes too thick for the electrons to penetrate, precluding any MicroED measurements. Strategies for diluting the thick lipid matrix around crystals were recently described using soluble proteins, but, when applied to membrane proteins, the quality of the crystals rapidly deteriorated, resulting in low-resolution data at best (14).

The voltage-dependent anion channel (VDAC) is a mammalian membrane protein that resides on the mitochondrial outer

Significance

Microcrystal electron diffraction (MicroED) is an electron cryomicroscopy (cryoEM) method for determining structures using submicron crystals. Until now, determining structures of membrane proteins by MicroED required that the protein crystals be in a solution amenable to standard cryoEM blotting and vitrification protocols. Here, we show that membrane protein microcrystals grown in a viscous bicelle mixture can become amenable to MicroED analyses by using modified blotting procedures combined with focused ion-beam milling. Our findings provide a basis for solving membrane protein structures using crystals embedded in a viscous media by MicroED.

Author contributions: J.A. and T.G. designed research; M.W.M., F.K., and J.H. performed research; M.W.M. collected the MicroED data; F.K. and J.A. contributed new reagents; M.W.M., F.K., J.H., and T.G. analyzed data; and M.W.M. and T.G. wrote the paper with input from all authors.

The authors declare no competing interest.

This article is a PNAS Direct Submission.

[1]To whom correspondence may be addressed. Email: tgonen@g.ucla.edu.

This article contains supporting information online at https://www.pnas.org/lookup/suppl/doi:10.1073/pnas.2020010117/-/DCSupplemental.

First published December 8, 2020.

membrane. Traditionally, VDAC crystals have been studied in detergent (15, 16) and within a lipid matrix (17–19) by X-ray crystallography in apo and adenosine triphosphate-bound forms. The 31 kDa polypeptide has a short amino (N)-terminal α-helix surrounded by a 19-stranded β-barrel–forming hydrophilic pore that allows cargo up to 5 kDa in size to traverse the mitochondrial membrane. These structural blueprints facilitated additional biochemical analyses that have identified cholesterol neurosteroid-binding sites (20) and have determined the unique roles of individual amino acids (21–23). Crystallization efforts aimed at determining the structure of a novel K12E mutant mVDAC (referred to as mVDAC hereafter) protein in lipid bicelles were stymied because only small crystals, almost indistinguishable by eye, were obtained. Efforts to increase their size were unsuccessful, making this an ideal specimen for investigation by MicroED.

Samples in MicroED are prepared similarly to other modalities of cryoEM (24, 25). Briefly, a small amount of liquid is added to an electron microscopy (EM) grid. The grid is gently blotted to remove the excess solvent, vitrified in liquid ethane, and stored in liquid nitrogen for future investigation. In the past, only crystals that happened to be very thin (<500 nm) or could be fragmented by sonication or vortexing were amenable to MicroED data-collection strategies (26, 27). Unfortunately, membrane protein crystals rarely grow thin enough for MicroED. These crystals tend to be more delicate and do not survive the harsh sonication/vortexing treatment, necessitating new sample-preparation methods. Recently, the use of a focused-ion beam (FIB) on a scanning-electron microscope (SEM) was demonstrated as a viable sample preparation technique for MicroED (28–30) (Fig. 1). With this method, an SEM is used to identify crystals, and a FIB is used to thin the crystals to <500 nm thickness, creating the ideal samples for MicroED. Two recent reports describe attempts to determine the MicroED structures of a membrane protein embedded in LCP, but neither was successful, likely because of suboptimal sample-preparation methods (14, 31). Importantly, structure determination by MicroED of FIB-milled crystals has, to date, only been successful for soluble proteins, such as lysozyme and proteinase K (28–30, 32–35).

Here, we demonstrate the application of FIB milling on membrane protein crystals of mVDAC grown in lipid bicelles. Three mVDAC crystals embedded in thick bicelle media were located in the FIB/SEM and milled into 200 nm-thick lamellae. MicroED data were collected and merged to 80% completeness at 3.1 Å resolution. The structure of mVDAC was solved by molecular replacement using a wild-type VDAC model (Protein Data Bank [PDB] ID code 3EMN) (19). Evidence for lipid packing between mVDAC monomers was visible in the density maps. Our results demonstrate that membrane protein crystals embedded in dense, viscous media can be made amenable to MicroED investigation by cryoFIB milling, increasing the scope

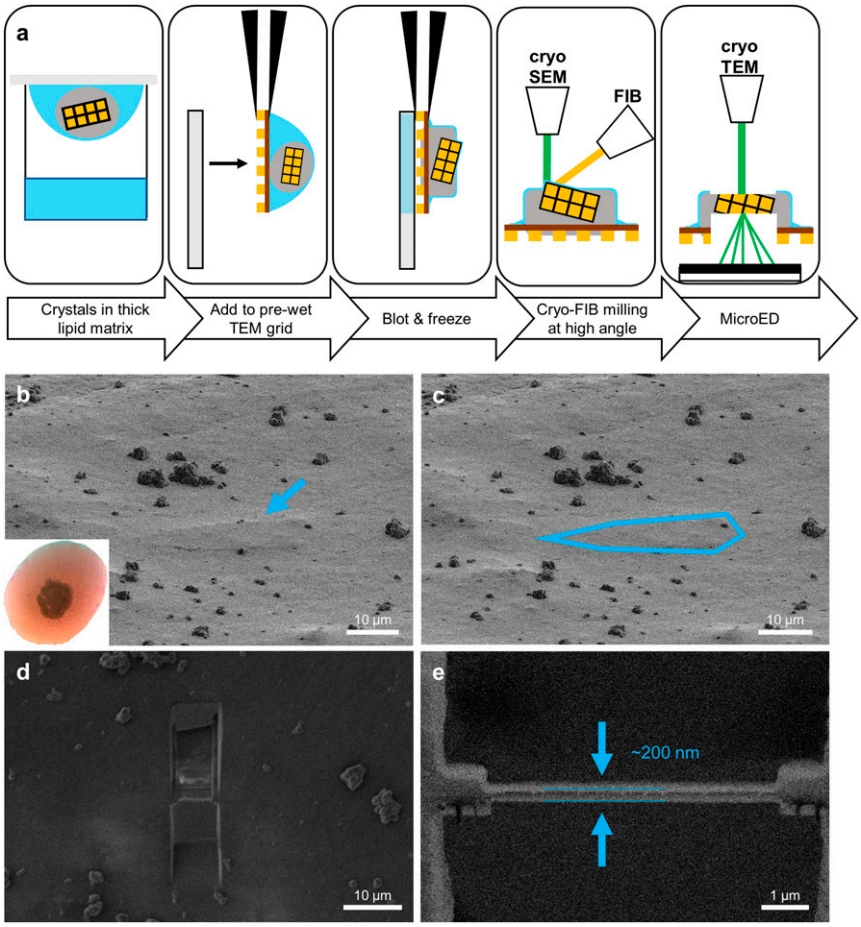

Fig. 1. Preparing viscous samples for cryoFIB and MicroED. (*A*) Schematic cartoon demonstrating the steps in the pipeline for studying membrane protein crystals grown in a lipid matrix by MicroED. (*B* and *C*) FIB image of an identified crystal prior to milling (arrow) (*B*) and this same picture with the thin crystal outlined in blue (*C*). (*D*) SEM image of the final crystalline lamellae milled at 30° showing stratification between the deposited platinum layer, crystal, and thick bicelle media. (*E*) FIB image of the final lamellae in the FIB used to measure thickness. mVDAC crystals were about 200 nm thick. Lines indicate top and bottom of lamella. The crystallization drop with bicelle solution is shown in *B*, *Inset*.

of the method to include more challenging and biologically important membrane proteins grown in a lipid matrix.

Results and Discussion

Crystals of mVDAC were grown in bicelles as previously described (19). In this condition, only very small and thin plate-shaped microcrystal shards formed within a dense core of a thick and viscous lipid matrix (Fig. 1, *Inset*). Despite significant effort, we were unable to grow larger crystals for X-ray crystallography and therefore decided to explore the use of MicroED.

Preparing grids of mVDAC for MicroED proved to be challenging because of the lipid matrix in the crystallization drops. These were viscous and difficult to handle. The steps we took for optimizing sample preparation for MicroED of the mVDAC crystals in the lipid matrix are documented in *SI Appendix*. The grid preparation improved with each step, leading to higher-quality data (*SI Appendix*) with an increasing signal-to-noise ratio (*SI Appendix*). We first attempted to prepare grids for MicroED by depositing an entire bicelle drop onto the TEM grid and gently blotting from the opposite side, as previously described for soluble protein crystals (36). These attempts resulted in samples that were too thick and could not be penetrated by the electron beam. To overcome these limitations, we used FIB/SEM to thin the crystalline material and its surrounding to thicknesses that are tractable for MicroED. Maintaining the grids in a humidity chamber held at ∼35% during blotting resulted in grids with large amorphous material and no visible crystals. Blotting from the front and the back typically broke the windows, and all crystalline material was lost. Grids with less amorphous material, but visible crystal edges, were identified by adding mother liquor to the grid prior to blotting at ambient humidity and then rinsing the grids with additional mother liquor before secondary blotting. This additional washing step allowed us to discover crystals previously hidden underneath the thick lipid bicelle material, but it resulted in poor or no diffraction. We surmise that the crystal lattice was damaged by the harsh treatment.

The breakthrough for MicroED sample preparation occurred when the crystals were kept hydrated. We added additional mother liquor on top of the crystal drops to reduce evaporation and minimize lipid exposure to environmental air. In addition, the cryoEM grid was wetted with 2 μL of mother liquid inside of a vitrification robot operating at 4 °C and 90% humidity to limit dehydration during sample application. Approximately 0.5 μL of the central crystal/lipid matrix was carefully pipetted onto the wet grid. The sample was incubated for 20 s and then gently blotted—from behind—and immediately plunged into supercooled liquid ethane for vitrification. Grids were transferred under cryogenic conditions to a cryoFIB/SEM for further investigation. Grids with mVDAC crystals were inspected by SEM. Upon visual inspection, the grid appeared to be covered by a thick layer of deposit that impeded crystal identification (Fig. 1*B*). Upon careful inspection at high magnification, thin mVDAC crystals were observed under a thick lipid matrix (arrow in Fig. 1*B* and outline in Fig. 1*C*).

The mVDAC crystals were milled similarly to previous reports (29, 30) but with important modifications. We noticed that the viscosity and thickness of the lipid matrix afforded considerable challenges. It was key to minimize damage to the underlying crystalline lattice during milling. To determine the total thickness of the preparation, we first milled trenches—in front of and behind—the target crystal at a high angle of 35° compared to the minimum milling angle of 12°. The high milling angle facilitated the examination of the specimen to determine the milling trajectory and strength (Fig. 1*C*). After trenching, three mVDAC crystals were milled at a maximum angle of 30°. The milling angle was adjusted to ensure the crystals would be accessible after rotating the grid for inspection in the TEM. Milling was conducted in sections either above or below the crystal for short periods of time using low currents to prevent overheating the sample and damaging the lattice (*Materials and Methods*). We observed that even short bursts of higher currents would overexpose the crystals, destroying the underlying lattice and resulting in little or no diffraction. This observation is in sharp contrast to crystals of soluble proteins that appear to provide atomic-resolution data even when exposed to much greater currents (30). Therefore, to minimize radiation damage to membrane protein crystals, the ion-beam current was ramped down in steps as milling progressed (29, 30). After a polishing step, thin crystalline lamellae that were ∼200 nm thick were obtained (Fig. 1*E*). The preparation was transferred to a cryoTEM for MicroED data collection.

MicroED Data Collection, Analysis, and Structure Determination. The milled lamellae were loaded into a 300kV Titan Krios transmission electron microscope (TEM) equipped with a CetaD complementary metal oxide semiconductor (CMOS) camera. Lamellae were easy to identify in the TEM: they appeared as a bright stripe against an otherwise dark background (Fig. 2, *Inset*). Five hydrated mVDAC lamellae were tested in the Titan Krios, and three of them diffracted to ∼3Å resolution (Fig. 2). We were able to cover a large portion of the reciprocal space per crystal lamella (Movie S1).

The continuous-rotation MicroED data were saved as MRC files and converted to SMV format using an in-house program that is freely available (https://cryoem.ucla.edu/MicroED). Images were then processed in XDS (37), with the negative pixels being lifted using a pedestal of 512 ADU as previously described (38, 39). The space group was identified to be C 1 2 1, with a unit cell of (a, b, c) = (98.9, 58.21, 69.54), and (α, β, γ) = (90, 99.44, 90), which is very similar to the parameters of the wild-type mVDAC (19). A resolution cutoff was applied at 3.1 Å, with an overall completeness of 80% (Table 1). Merging data from additional crystals did not increase the completeness due to the

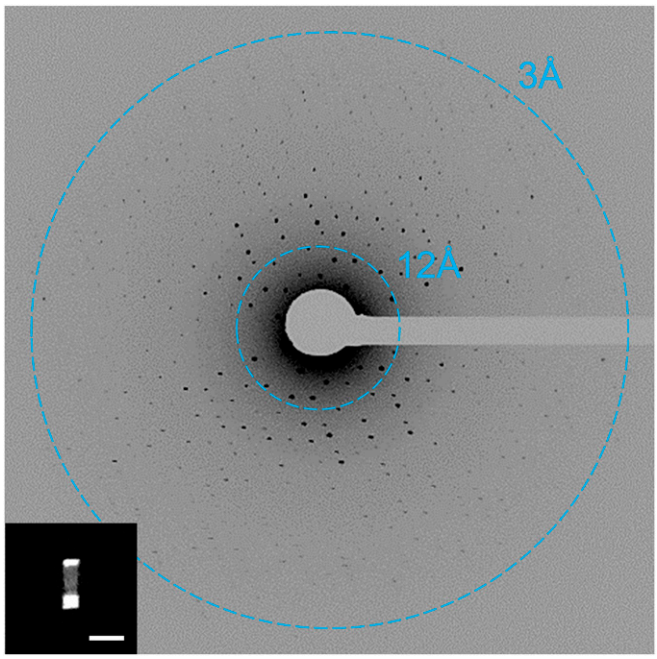

Fig. 2. MicroED data from VDAC lamellae. A maximum projection through 10 degrees of a MicroED dataset. Strong reflections are easily observed to approximately 3Å resolution. (*Inset*) TEM micrograph of crystal lamella used for the data shown. (Scale bar is 10 μm.)

Table 1. MicroED crystallographic table

mVDAC data processing statistics	Value
mVDAC integration statistics	
Wavelength (Å)	0.0197
Resolution range (Å)	29.1 to 3.1
Space group	C 1 2 1
Unit cell (a, b, c) (Å)	98.9, 58.2, 69.5
(α, β, γ) (°)	90.0, 99.4, 90.0
Total reflections (no.)	32,641
Multiplicity	5.8
Completeness (%)	80.1
Mean $I/\sigma(I)$	2.29
R_{pim}	0.22
$CC_{1/2}$	0.92
Refinement statistics	
R_{work}	0.2565
R_{free}	0.2870
Protein residues (no.)	283
rms (bonds)	0.002
rms (angles)	0.585
Ramachandran favored (%)	86.48
Ramachandran allowed (%)	11.03
Ramachandran outliers (%)	2.49
Rotamer outliers (%)	0.43
Clash score	6.49

preferred orientation of the mVDAC crystals on the grid. Similar phenomena were observed for catalase crystals, which also formed flat plates and had a preferential orientation (40). The structure of mVDAC was solved by molecular replacement using the wild-type model of VDAC (PDB ID code 3EMN) (19). A single solution was found with a translational Z score and log-likelihood gain of 19.6 and 960, respectively. Following molecular replacement, the structure was inspected in Coot (41) and refined.

Refinement of mVDAC followed standard procedures (25, 39). The model from molecular replacement was refined using electron-scattering factors in phenix.refine (42). Refinement was iterated with visual inspection, eventually resulting in R_{work} and R_{free} of 25.65% and 28.70%, respectively. The final model of mVDAC contained an N-terminal α-helix surrounded by a bundle of 19 β-strands forming a barrel that encloses a hydrophilic pore (Fig. 3*A* and *SI Appendix*). This structure is similar to the wild-type mVDAC with an all-atom rmsd of less than 1 Å^2.

The packing of mVDAC monomers within the crystal lattice involved direct protein–protein contacts as well as contacts likely mediated by lipids. The different contact sites exist because individual mVDAC barrels do not pack as a planar hexagonal lattice as one would predict for a round monomer. Instead, each monomer makes close contacts with three monomers and more distant contacts with an additional four monomers in a planar arrangement (Fig. 3*B*). The three nearest neighbors of an mVDAC monomer are close enough for direct protein–protein crystal contacts, but the other four neighboring barrels are too far, separated by up to 34 Å from one another. The space between these distant mVDAC barrels is likely filled with lipids that mediate crystal-packing interactions (Fig. 3*B*). At this stage, we chose not to model the lipids as we only observed discontinuous density for the lipid moieties. We note that lipids have been observed to mediate crystal contacts in other membrane proteins, notably aquaporin-0, but were only fully resolved and modeled at higher resolutions (43, 44).

Here, we resolved a structure of a mammalian membrane protein grown in a lipid environment that was not tractable by other crystallographic methods. While wild-type VDAC readily grows large crystals suitable for X-ray crystallography, the crystals of the essential mutant— studied here—were scarcely visible and not amenable to analysis by X-ray crystallography. These crystals grew in a thick lipid matrix that made isolating crystals for MicroED challenging. In this case, FIB milling was used to remove excess material and allow structure determination by MicroED once crystal hydration was maintained during grid preparation. The MicroED structure was solved from three milled crystals, each less than 1 μm^3, which would not have been possible using synchrotron X-ray crystallography. Finally, as future studies will focus on improving the resolution of this approach, we expect to fully resolve the lipids that mediate crystal contacts in mVDAC and other crystals of membrane proteins grown in a lipid matrix. This combination of methodologies could allow MicroED to be successfully employed for investigating the influence of lipids on novel membrane protein structures in ways that were previously not possible.

Materials and Methods

Protein Production and Purification. Lipid bicelles were prepared as previously described (3). Mutant K12E VDAC (referred to as mVDAC herein) was expressed and purified, as described for wild-type VDAC (19). Protein was concentrated to 15 mg/mL and mixed in a 4:1 protein/bicelle ratio resulting in 12 mg/mL mVDAC1 in 7% bicelles.

Protein Crystallization. Crystal screens for mVDAC were started from the known wild-type VDAC crystallization conditions at 20 °C (19). Microcrystals in bicelles appeared in a well containing 20% 2-methyl-2,4-pentandiol and 0.1 M tris(hydroxymethyl)aminomethane·HCl (pH 8.5) with 10% polyethylene glycol 400 added to the protein drop only.

Grid Preparation. This procedure describes the preparation that gave rise to the final structure. Other conditions that were tested are described in *SI Appendix*. Quantifoil R2/2 Cu200 grids were glow-discharged for 30 s prior to use. The blotting chamber was set to 4 °C and 90% humidity, and filter paper was added. The system was allowed to equilibrate for 15 min before any blotting was conducted; 2 μL of mother liquid was added to the grid inside of a vitrification robot to prevent any dehydration during application. A small portion (0.5 μL) from the central lipid clump within the crystallization drop was carefully pipetted into the already-applied 2 μL of mother liquor. The sample chamber of the vitrification robot was held at 90% humidity. This mixture was allowed to incubate for 20 s and was then gently blotted from the back and immediately vitrified in liquid ethane as described (36). Grids were stored in liquid nitrogen prior to further investigation.

CryoSEM Imaging and CryoFIB Milling of VDAC. All FIB/SEM experiments were performed using a Thermo-Fisher Aquilos dual-beam FIB/SEM instrument at liquid nitrogen temperatures, as described (28–30, 34) but modified as follows. The instrument was operated at 2 kV and 3.1 pA while using the SEM for imaging and 30 kV and 1.5 or 10 pA while operating the FIB for imaging. All ion-beam milling was conducted at an accelerating voltage of 30 kV. The grid was sputter-coated in platinum for 1 min using a high current in order to evenly cover the entire grid under a 500 nm-thick layer of platinum. An all-grid map was collected in the Maps software (Thermo-Fisher), where potential crystals were identified by looking for sharp edges in areas not overlapping the grid bars. Each grid square was individually inspected again using the FIB at 1.5- to 10-pA current to verify the already-selected crystals or identify new crystals. Verified mVDAC crystals were brought to eucentric height prior to milling. Milling was conducted as described (29, 30, 36). In general, milling was done in batch, where each step of rough, fine, and ultrafine milling (or polishing) was conducted on each crystal prior to additional thinning. In this way, contamination of the lamellae by amorphous ice was minimized. Milling lamellae began by removing large wedges of material above and below the crystal by cleaning rectangular cross-sections between 5 and 10 μm across and 5 μm tall. These rectangles started 10 to 15 μm apart, and this rough initial milling was conducted at an ion-beam current of 300 pA. After inspection, the size of the rectangles was reduced, having the same width but now only 2 μm in height. From here, the distance between the rectangles was reduced in steps of 2 μm such that 1 μm of material was removed from either the top or the bottom of the crystal and/or the grid. These cleaning cross-section steps were conducted at a beam current of 100 pA until the lamellae were reduced to a total thickness of 2 μm. At this point, the rectangular section width was reduced by 1 to 4 μm,

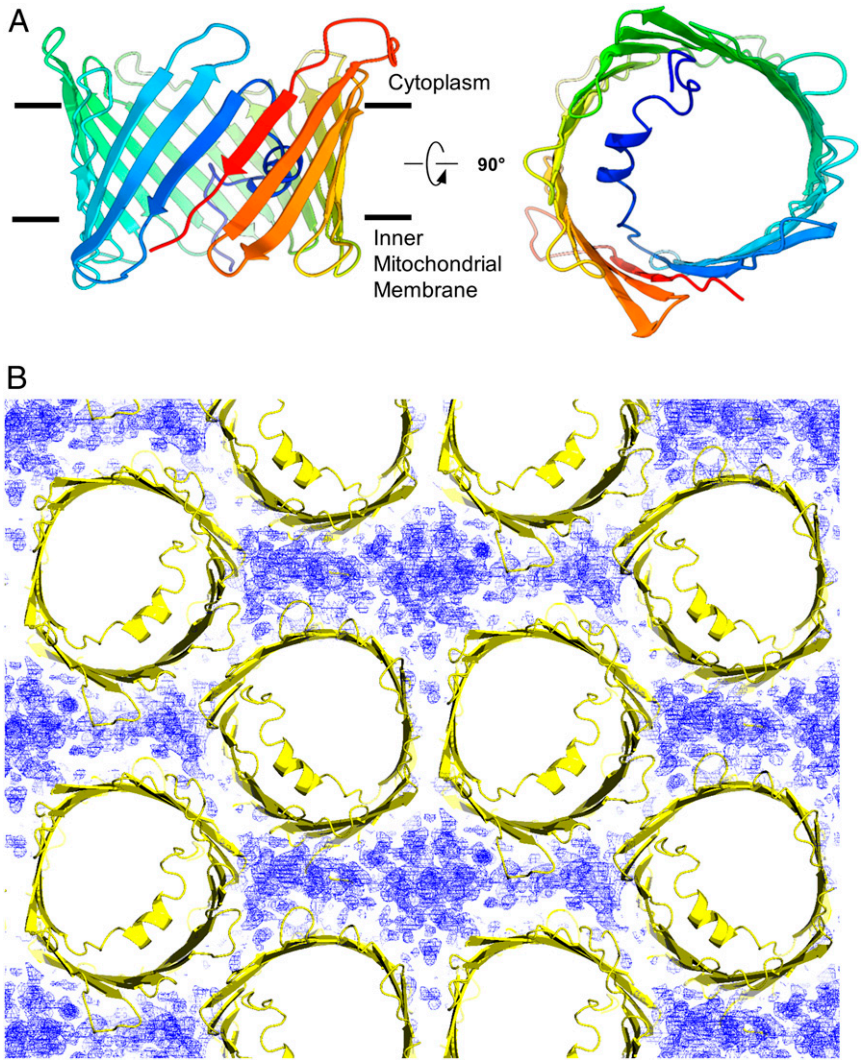

Fig. 3. The structure and packing of mVDAC by MicroED. (*A*) The final structure of mVDAC at 3.1Å resolution in side and top views (*Left* and *Right*, respectively). (*B*) The $2F_o$-F_c map in blue displayed in the regions between protein monomers displayed in yellow. The map is shown at the 0.5σ level.

and the height was reduced to 1 μm. Cleaning cross-sections, removing material from the top and bottom of the grid, were conducted to reduce the size of the lamellae to ∼500 nm. The rectangle size was reduced again by ∼1 μm in width and to 500 nm in height. Cleaning cross-sections were conducted to reduce the lamellae to ∼300 to 400 nm. These steps were conducted at an ion-beam current of 50 pA. Upon inspection, these lamellae were thinned by drawing rectangles just above and below the coarsely milled lamellae of ∼100 nm in height and matched the approximate width of the lamellae. These rectangles were set to overlap by 50 nm on both the top and bottom sides of the crystal. These rectangles were milled in normal cross-sections at an ion-beam current of 10 pA until material could no longer be seen within either rectangle by adjusting the contrast of the images.

MicroED Data Collection. Data collection was performed as described (24, 29, 39, 45). MicroED was tested on a 200-kV Talos Arctica equipped with a CetaD CMOS-based camera (Thermo-Fisher). Individual diffraction patterns were collected from each lamella without rotation to evaluate the quality of diffraction that could be obtained. Data were then collected on a cryocooled Titan Krios operating at 300 kV, corresponding to an electron wavelength of 0.0197 Å. The Titan Krios was similarly equipped with a CetaD CMOS-based camera. Lamellae were identified in low-magnification montage taken at ∼64× magnification. Data were collected under continuous rotation from the three lamellae at rotation speeds between 0.1 and 0.3 ° s^{-1}, with frames being read out at every 5, 3, and 2 s. The general strategy was to collect data with individual wedges corresponding to ∼0.5°. The exposure rate was set to less than 0.01 e^- $Å^{-2}$ s^{-1} to limit radiation damage (46). Data were recorded using a selected area aperture that limited the recordable area to a region ∼2 μm in diameter. Since the lamella thickness was ∼200 nm, each MicroED dataset was collected from a crystalline volume of less than 1 $μm^3$. Data were saved as single MRC stacks prior to analysis.

MicroED Data Processing. Data were converted from MRC to SMV format using software that is freely available (https://cryoem.ucla.edu/). Converted frames were used to index, integrate, and scale the data in XDS and XSCALE (37, 47). Individual datasets were optimized by removing frames from the end to improve the scaling between the three datasets. The collected rotation ranges for the three datasets were −60 to +56°, +68 to −45°, and −54 to +58°. Each of these ranges were then cut to improve the merging statistics, yielding final merged wedges of −60 to +15°, +68 to −17°, and −16 to 56°. The merged datasets therefore covered a rotation range spanning −60 to +68°. A resolution cutoff was applied at 3.1 Å, where the $CC_{1/2}$ of the merged data remained positive. Further optimization of the resolution cutoff was not attempted. Molecular replacement was performed in PHASER (48) using the PDB ID code 3EMN (19). A single solution was identified in space group C 1 2 1. The initial model from PHASER was inspected in Coot (41) prior to refinement. Refinement was conducted in phenix.refine using electron-scattering factors (49). The structure was left as is without further modeling any densities outside of the protein residues, as these are to be detailed in future work regarding the functional importance of this mutation.

Data Availability. The structure factors and coordinates have been deposited in the PDB [PDB ID code 7KUH (50)] and the associated map in the Electron Microscopy Data Bank [EMDB ID code EMD-23037 (51)].

ACKNOWLEDGMENTS. The Gonen laboratory is supported by funds from the Howard Hughes Medical Institute. This study was supported by NIH Grants P41GM136508 (to T.G.) and R35 GM135175 (to J.A.).

1. C. Hunte, S. Richers, Lipids and membrane protein structures. *Curr. Opin. Struct. Biol.* **18**, 406–411 (2008).
2. V. Cherezov, Lipidic cubic phase technologies for membrane protein structural studies. *Curr. Opin. Struct. Biol.* **21**, 559–566 (2011).
3. S. Faham, J. U. Bowie, Bicelle crystallization: A new method for crystallizing membrane proteins yields a monomeric bacteriorhodopsin structure. *J. Mol. Biol.* **316**, 1–6 (2002).
4. E. M. Landau, J. P. Rosenbusch, Lipidic cubic phases: A novel concept for the crystallization of membrane proteins. *Proc. Natl. Acad. Sci. U.S.A.* **93**, 14532–14535 (1996).
5. R. Ujwal, J. Abramson, High-throughput crystallization of membrane proteins using the lipidic bicelle method. *J. Vis. Exp.* e3383 (2012).
6. R. B. G. Ravelli *et al*., Cryo-EM structures from sub-nl volumes using pin-printing and jet vitrification. *Nat. Commun.* **11**, 2563 (2020).
7. J. Zhao, *et al*., A simple pressure-assisted method for cryo-EM specimen preparation. bioRxiv. https://doi.org/10.1101/665448 (2019).
8. Y. Z. Tan, J. L. Rubinstein, Through-grid wicking enables high-speed cryoEM specimen preparation. bioRxiv. https://doi.org/10.1101/2020.05.03.075366 (4 May 2020).
9. L. Zhu *et al*., Structure determination from lipidic cubic phase embedded microcrystals by MicroED. *Structure* **28**, 1149.e4–1159.e4 (2020).
10. K. Yonekura, K. Kato, M. Ogasawara, M. Tomita, C. Toyoshima, Electron crystallography of ultrathin 3D protein crystals: Atomic model with charges. *Proc. Natl. Acad. Sci. U.S.A.* **112**, 3368–3373 (2015).
11. S. Liu, T. Gonen, MicroED structure of the NaK ion channel reveals a Na^+ partition process into the selectivity filter. *Commun. Biol.* **1**, 38 (2018).
12. J. Dubochet, M. Adrian, J. Lepault, A. W. McDowall, Emerging techniques: Cryo-electron microscopy of vitrified biological specimens. *Trends Biochem. Sci.* **10**, 143–146 (1985).
13. Q.-X. Jiang, T. Gonen, The influence of lipids on voltage-gated ion channels. *Curr. Opin. Struct. Biol.* **22**, 529–536 (2012).
14. L. Zhu *et al*., Structure determination from lipidic cubic phase embedded microcrystals by MicroED. *Structure* **28**, 1149.e4–1159.e4 (2020).
15. M. Bayrhuber *et al*., Structure of the human voltage-dependent anion channel. *Proc. Natl. Acad. Sci. U.S.A.* **105**, 15370–15375 (2008).
16. T. Meins, C. Vonrhein, K. Zeth, Crystallization and preliminary X-ray crystallographic studies of human voltage-dependent anion channel isoform I (HVDAC1). *Acta Crystallogr. Sect. F Struct. Biol. Cryst. Commun.* **64**, 651–655 (2008).
17. O. P. Choudhary *et al*., Structure-guided simulations illuminate the mechanism of ATP transport through VDAC1. *Nat. Struct. Mol. Biol.* **21**, 626–632 (2014).
18. J. Schredelseker *et al*., High resolution structure and double electron-electron resonance of the zebrafish voltage-dependent anion channel 2 reveal an oligomeric population. *J. Biol. Chem.* **289**, 12566–12577 (2014).
19. R. Ujwal *et al*., The crystal structure of mouse VDAC1 at 2.3 A resolution reveals mechanistic insights into metabolite gating. *Proc. Natl. Acad. Sci. U.S.A.* **105**, 17742–17747 (2008).
20. W. W. L. Cheng *et al*., Multiple neurosteroid and cholesterol binding sites in voltage-dependent anion channel-1 determined by photo-affinity labeling. *Biochim. Biophys. Acta Mol. Cell Biol. Lipids* **1864**, 1269–1279 (2019).
21. L. A. Bergdoll *et al*., Protonation state of glutamate 73 regulates the formation of a specific dimeric association of mVDAC1. *Proc. Natl. Acad. Sci. U.S.A.* **115**, E172–E179 (2018).
22. V. Betaneli, E. P. Petrov, P. Schwille, The role of lipids in VDAC oligomerization. *Biophys. J.* **102**, 523–531 (2012).
23. T. K. Rostovtseva, S. M. Bezrukov, VDAC regulation: Role of cytosolic proteins and mitochondrial lipids. *J. Bioenerg. Biomembr.* **40**, 163–170 (2008).
24. B. L. Nannenga, D. Shi, A. G. W. Leslie, T. Gonen, High-resolution structure determination by continuous-rotation data collection in MicroED. *Nat. Methods* **11**, 927–930 (2014).
25. D. Shi *et al*., The collection of MicroED data for macromolecular crystallography. *Nat. Protoc.* **11**, 895–904 (2016).
26. M. J. de la Cruz *et al*., Atomic-resolution structures from fragmented protein crystals with the cryoEM method MicroED. *Nat. Methods* **14**, 399–402 (2017).
27. M. W. Martynowycz *et al*., MicroED structures from micrometer thick protein crystals. *BioRxiv*. 2017 Jan 1:152504. DOI: https://doi.org/10.1101/152504.
28. H. M. E. Duyvesteyn *et al*., Machining protein microcrystals for structure determination by electron diffraction. *Proc. Natl. Acad. Sci. U.S.A.* **115**, 9569–9573 (2018).
29. M. W. Martynowycz, W. Zhao, J. Hattne, G. J. Jensen, T. Gonen, Collection of continuous rotation MicroED data from ion beam-milled crystals of any size. *Structure* **27**, 545.e2–548.e2 (2019).
30. M. W. Martynowycz, W. Zhao, J. Hattne, G. J. Jensen, T. Gonen, Qualitative analyses of polishing and precoating FIB milled crystals for MicroED. *Structure* **27**, 1594.e2–1600.e2 (2019).
31. V. Polovinkin *et al*., Demonstration of electron diffraction from membrane protein crystals grown in a lipidic mesophase after lamella preparation by focused ion beam milling at cryogenic temperatures. *J. Appl. Cryst.* **53**, (2020).
32. E. V. Beale *et al*., A Workflow for Protein Structure Determination From Thin Crystal Lamella by Micro-Electron Diffraction. *Front. Mol. Biosci.* **7**, 179, 10.3389/fmolb.2020.00179 (2020).
33. X. Li, S. Zhang, J. Zhang, F. Sun, *In situ* protein micro-crystal fabrication by cryo-FIB for electron diffraction. *Biophys. Rep.* **4**, 339–347 (2018).
34. A. M. Wolff *et al*., Comparing serial X-ray crystallography and microcrystal electron diffraction (MicroED) as methods for routine structure determination from small macromolecular crystals. *IUCrJ* **7**, 306–323 (2020).
35. H. Zhou, Z. Luo, X. Li, Using focus ion beam to prepare crystal lamella for electron diffraction. *J. Struct. Biol.* **205**, 59–64 (2019).
36. Michael W. Martynowycz, Tamir Gonen, Ligand Incorporation into Protein Microcrystals for MicroED by On-Grid Soaking. *Structure*, 10.1016/j.str.2020.09.003 (2020).
37. W. Kabsch, XDS. *Acta Crystallogr. D Biol. Crystallogr.* **66**, 125–132 (2010).
38. J. Hattne, D. Shi, M. J. de la Cruz, F. E. Reyes, T. Gonen, Modeling truncated pixel values of faint reflections in MicroED images. *J. Appl. Cryst.* **49**, 1029–1034 (2016).
39. J. Hattne *et al*., MicroED data collection and processing. *Acta Crystallogr. A Found. Adv.* **71**, 353–360 (2015).
40. B. L. Nannenga, D. Shi, J. Hattne, F. E. Reyes, T. Gonen, Structure of catalase determined by MicroED. *eLife* **3**, e03600 (2014).
41. P. Emsley, K. Cowtan, *Coot*: Model-building tools for molecular graphics. *Acta Crystallogr. D Biol. Crystallogr.* **60**, 2126–2132 (2004).
42. P. V. Afonine *et al*., Towards automated crystallographic structure refinement with phenix.refine. *Acta Crystallogr. D Biol. Crystallogr.* **68**, 352–367 (2012).
43. T. Gonen *et al*., Lipid-protein interactions in double-layered two-dimensional AQP0 crystals. *Nature* **438**, 633–638 (2005).
44. T. Gonen, P. Sliz, J. Kistler, Y. Cheng, T. Walz, Aquaporin-0 membrane junctions reveal the structure of a closed water pore. *Nature* **429**, 193–197 (2004).
45. D. Shi, B. L. Nannenga, M. G. Iadanza, T. Gonen, Three-dimensional electron crystallography of protein microcrystals. *eLife* **2**, e01345 (2013).
46. J. Hattne *et al*., Analysis of global and site-specific radiation damage in cryo-EM. *Structure* **26**, 759–766.e4 (2018).
47. W. Kabsch, Integration, scaling, space-group assignment and post-refinement. *Acta Crystallogr. D Biol. Crystallogr.* **66**, 133–144 (2010).
48. A. J. McCoy *et al*., *Phaser* crystallographic software. *J. Appl. Cryst.* **40**, 658–674 (2007).
49. P. D. Adams *et al*., The Phenix software for automated determination of macromolecular structures. *Methods* **55**, 94–106 (2011).
50. M. W. Martynowycz, F. Khan, J. Hattne, J. Abramson, T. Gonen, MicroED structure of mVDAC. Protein Data Bank. https://www.rcsb.org/structure/7KUH. Deposited 24 November 2020.
51. M. W. Martynowycz, F. Khan, J. Hattne, J. Abramson, T. Gonen, MicroED structure of mVDAC. Electron Microscopy Data Bank. https://www.ebi.ac.uk/pdbe/entry/emdb/EMD-23037. Deposited 24 November 2020.